Sum-Rate Maximization of Symbiotic Multi-V2X MISO and Multi-RIS BackCom with Imperfections

Derek Kwaku Pobi Asiedu, Kofi Ofori-Amanfo, Mustapha Benjillali, Ji-Hoon Yun, Samir Saoudi

Sum-Rate Maximization of Symbiotic Multi-V2X MISO and Multi-RIS BackCom with Imperfections

Derek K. P. Asiedu*, Kofi A. Ofori-Amanfo†, Mustapha Benjillali‡*, Ji-Hoon Yun†, and Samir Saoudi*
*IMT-Atlantique, Lab-STICC, 29238 Brest, France. Emails: kwakupobi@ieee.org, and samir.saoudi@imt-atlantique.fr
†Department of Electrical and Information Engineering, SeoulTech, Seoul 01811, South Korea. Email: jhyun@seoultech.ac.kr
‡Department of Communication Systems, INPT, Rabat 10100, Morocco. Email: benjillali@ieee.org

***Abstract*—In this paper, we develop an optimization framework for the symbiotic operation of a primary multi-vehicle-to-everything (MV2X) communication network employing downlink communication and a secondary backscatter (BC) communication (BackCom) network of wireless-powered sensor equipped reflecting configurable surfaces (RISs), sharing the same spectrum. The secondary semi-passive RISs provide the multiple primary receivers with a spatial diversity gain and enable transmitting their own data to a designated IoT central system equipped with a BC reader. We develop an alternating optimization algorithm for resource allocation to maximize the sum-rate for mutually beneficial symbiotic radio operation. The presented simulation results demonstrate the superiority of the proposed optimization algorithm over conventional beamforming designs and fixed RIS reflection coefficient benchmarks.**

***Index Terms*—Symbiotic radio network (SRN), sum-rate (SR), backscatter communication (BackCom), resource allocation.**

I. Introduction

The ongoing paradigm shifts in Internet-of-things networks (IoTNs) and next-generation wireless communication [1] consider the following key objectives. (i) Enhancement of current IoTN architectures to facilitate larger connectivity, reduce network latency, and improve network reliability. (ii) Implementation of novel communication techniques for large simultaneous connectivity, efficient use of network resources, and extension of network coverage. (iii) Exploration of new spectrum resources and efficient management of already allocated ones. These innovative solutions are applicable to traditional cellular, industrial, environmental monitoring, precision farming, and vehicle-to-everything (V2X) communication networks [2].

Among the triad of concerns, the preeminent issue revolves around spectrum usage and management since the spectrum resource is scarce. The scarce spectrum resource must be allocated amongst various types of networks, including V2X communication [1]. Therefore, current V2X communication standardization is geared towards the goal of efficient spectrum usage [2], which includes the move from fixed to dynamic and opportunistic spectrum access, and multiple instant simultaneous vehicle communication support [1].

This project received funding from the European Union's Horizon 2020 research and innovation programme under the Marie Skłodowska-Curie grant agreement No 899546 and in part from the Institute of Information Communications Technology Planning & Evaluation (IITP) Grant funded by the Korean Government (MSIT) under Grant 2022-0-00214.

A promising new and novel technique for efficient use and management of spectrum is symbiotic radio networks (SRNs), which is achieved through spectrum sensing and cognitive transmission [1]. This facilitates sharing and using the licensed V2X communication spectrum with underlying networks, such as environmental monitoring sensor networks. Simultaneously, the underlying unlicensed networks can leverage state-of-the-art data transmission backscatter communication (BackCom) technology. This is a technique, where a passive BackCom device equipped with a sensor transmits sensed data through *"backscattering"* Far-field radio frequency (RF) waves from a legitimate (licensed) spectrum user (transmitter) [3].

Multi-user non-orthogonal multiple access (MU-NOMA) technique is another new radio technology that has been proposed to help improve efficient spectrum use, management, and access. In this technique, a transmitter sends information simultaneously to multiple users over the same spectrum, with power allocation as the differentiating factor [1]. When applied to V2X communication, this approach allows multiple vehicles to connect to an access point over the same licensed spectrum simultaneously. A drawback of NOMA is the presence of inter-device interference, which can be mitigated by applying successive interference cancellation techniques (SIC). In addition, the far and near users within the MU-NOMA architecture can also benefit from deploying assistive technologies such as reconfigurable intelligent surfaces (RIS) deployment within the network to improve spatial diversity and network coverage.

Investigations have been conducted using various combinations of MU-NOMA and sensor-equipped RIS utilizing BackCom in SRN. Significantly, multi-V2X communications still need to be covered by these recent SRN developments with consideration of mobility and system imperfections, which hasn't been covered under SRNs. Focusing on primary network (PN) primary transmitter (PT) power minimization for a single primary receiver (PR) in a symbiotic relationship with a secondary transmitter (ST) sensor-equipped RIS in the presence of perfect (per) and imperfect channel state information (CSI) in discussed in [4]. An extension of [4] covering MIMO configuration in [5] for per-CSI. Further consideration of multi-PRs and MIMO secondary receiver (SR) BackCom reader of [4] is presented in [6]. The multi-PR and multi-RIS system model is considered in [7], which focuses on RIS-PR pairing and the maximization of the system-weighted

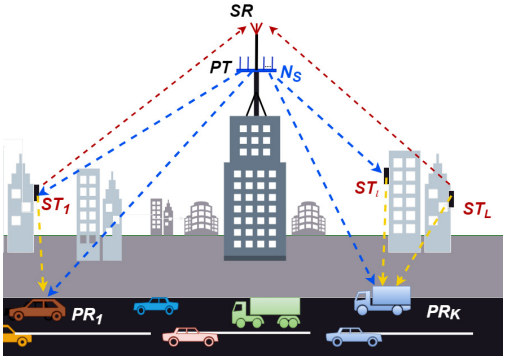

Fig. 1. A MV2X and SNSN SRN.

sum rate. A generalized case of all RISs and PRs sum-rate maximization in the presence of system imperfections is presented in [8]. These research outcomes, cements the need for more investigation into RISs-PRs focusing on system architecture, configuration and imperfections, and applications.

Motivation and Contribution: This paper considers sum-rate maximization for an Multi-V2X NOMA and multi-RIS BackCom SRN, which has not been considered in symbiotic radio research. Hence, the first motivation is the application of SRN within V2X communication and considering vehicle or device mobility in SRNs. The second contribution is efficiently allocating the newly proposed SRN in V2X communication resources to maximize the system sum-rate. Note that both the influence of the PN and SN rates are considered in the SR maximization problem similar to [9]. Finally, imp-CSI estimation and imp-SIC due to vehicle mobility, and estimation techniques imperfections are considered in this work [8].

Notations: bold and non-bold letters and symbols represent vector and scalar values. Superscript H represents transpose. $\mathcal{CN}(\mu, \Psi)$ represents a complex Gaussian distribution with mean μ and variance Ψ.

II. System Model and Problem Formulation

The considered SRN in this paper and shown in Fig. 1 consists of (i) a PN downlink (DL) N multi-antenna primary transmitter (PT) communicating with K multiple single-antenna vehicles (MV) (primary receivers (PRs)) using NOMA technique (called MV2X), and (ii) a SN including L multiple semi-passive RIS sensors (secondary transmitters (STs) with M_l reflective elements) backscattering (BackCom) sensed data to a single-antenna reader (secondary receiver (SR)) (called SNSN)[1]. The symbiotic relationship (mutual benefit) between the MV2X and SNSN is achieved through (i) the MV2X gaining spatial diversity from the STs backscattering the desired signals of the PRs (vehicles), (ii) while the SNSN uses the PT RF waves to excite the STs to transfer their sensed data to the reader (SR). An application of this SRN is a licensed band MV2X network underlined with a BackCom-enabled urban area environmental monitoring sensor network.

[1]Multi-antenna and rate-splitting will be considered in an extension of this paper, since this is an introduction of the SRN-V2X system mode.

The CSI estimation can be achieved using techniques from [8], [10]. It is assumed that there is imperfect (imp-) CSI due to vehicle mobility and the channels are estimated as $h_k[n] = \sqrt{\epsilon^2} h_k[n-1] + \sqrt{1-\epsilon^2} e_k[n]$, where $h_k[n] \sim \mathcal{CN}(0,1)$ is the current time (n) channel, $h_k[n-1] \sim \mathcal{CN}(0, 1-\sigma_e^2)$ is the channel estimated in the previous time $(n-1)$ (i.e., due to moving vehicle previous position and latency in CSI estimation), and $e_k[n] \sim \mathcal{CN}(0, \sigma_e^2)$ current channel estimation error [11]. $\epsilon = J_0(2\pi f_d T)$ is the time correlation component with $f_d = v f_c / C$ being the maximum Doppler frequency for carrier frequency f_c, vehicle speed v, and the speed of light C. T is the channel instantiation interval (delay in seconds) [11]. The signal decoding is accomplished through a combination of linear decoders and SIC [8], [12], with the undesired signals, $|\boldsymbol{\phi}_{l,k}^H \boldsymbol{\Theta}_l^{\frac{1}{2}} \tilde{\mathbf{H}}_l^H \mathbf{w}_j|^2 > |\boldsymbol{\phi}_{l,k}^H \boldsymbol{\Theta}_l^{\frac{1}{2}} \tilde{\mathbf{H}}_l^H \mathbf{w}_k|^2$, $|\mathbf{h}_k^H \mathbf{w}_j|^2 > |\mathbf{h}_k^H \mathbf{w}_k|^2$, $|\mathbf{h}_r^H \mathbf{w}_k|^2$, $|\boldsymbol{\phi}_{l,r}^H \boldsymbol{\Theta}_l^{\frac{1}{2}} \tilde{\mathbf{H}}_l^H \mathbf{w}_j|^2 > |\boldsymbol{\phi}_{l,r}^H \boldsymbol{\Theta}_l^{\frac{1}{2}} \tilde{\mathbf{H}}_l^H \mathbf{w}_k|^2$ treated as interference, but are cancelled vise versa during desired signal decoding. However, the SIC is assumed to be imperfect with a factor of $0 \leq \xi \leq 1$. The PT to SR signal can be removed using the RISscatter technique [12]. Here, $\mathbf{h}_k$, $\tilde{\mathbf{H}}_l$, $\mathbf{h}_r$, $\boldsymbol{\phi}_{l,k}$ and $\boldsymbol{\phi}_{l,r}$ are the PT to PR k, PT to ST l, PT to SR, ST l to PR k, and ST l to SR channels, respectively. $\boldsymbol{\Theta}_l = \text{diag}\{\eta_{1,l}, \ldots, \eta_{M_l,l}\}$ is ST l reflection co-efficient. $\mathbf{w}_k$ is the PT to PR l beamformer.

A. Signal Flow and Information Decoding Formulation

The received signal at PR k or SR is given as

$$y_{z_1,z_2} = \underbrace{n_k}_{\text{Antenna noise}} + \underbrace{\mathbf{h}_{z_2}^H \sum_{j=1}^{K} \mathbf{w}_j x_j}_{\text{DL direct signals}} + \underbrace{\sum_{l=1}^{L} \boldsymbol{\phi}_{l,z_2}^H \boldsymbol{\theta}_l^{\frac{1}{2}} \tilde{\mathbf{H}}_l^H \tilde{x}_l \sum_{j=1}^{K} \mathbf{w}_j x_j}_{\text{MV2X + SNSN BackCom signals}}, \quad (1)$$

$(z_1, z_2) \in \{(s,k), (l,r)\}$. After the desired signal decoding, PR k SINR and ST l SINR at SR are respectively derived as

$$\gamma_{s,k} = \frac{A_k}{B + C_k + \sigma_k^2}, \text{ and } \gamma_{l,r} = \frac{A_{l,r}}{B_{l,r} + C + \sigma_r^2}, \quad (2)$$

where $A_k = |\mathbf{h}_k^H \mathbf{w}_k|^2 + \sum_{l=1}^{L} |\boldsymbol{\phi}_{l,k}^H \boldsymbol{\Theta}_l^{\frac{1}{2}} \tilde{\mathbf{H}}_l^H \mathbf{w}_k|^2$ and $B = \sum_{l=1}^{L} \sum_{j=1}^{K} \xi_j |\boldsymbol{\phi}_{l,k}^H \boldsymbol{\Theta}_l^{\frac{1}{2}} \tilde{\mathbf{H}}_l^H \mathbf{w}_j|^2$ are PR k desired and the STs interference signals, respectively. $C_k = \sum_{j \neq k}^{K} |\mathbf{h}_j^H \mathbf{w}_j|^2 + \sum_{l=1}^{L} \sum_{j \neq k}^{K} \xi_j |\boldsymbol{\phi}_{l,k}^H \boldsymbol{\Theta}_l^{\frac{1}{2}} \tilde{\mathbf{H}}_l^H \mathbf{w}_j|^2$ is the other PRs interference signals. $A_{l,r} = \sum_{k=1}^{K} |\boldsymbol{\phi}_{l,r}^H \boldsymbol{\Theta}_l^{\frac{1}{2}} \tilde{\mathbf{H}}_l^H \mathbf{w}_k|^2$ and $B_{l,r} = \sum_{j \neq l}^{L} \sum_{k=1}^{K} \xi_j |\boldsymbol{\phi}_{j,r}^H \boldsymbol{\Theta}_j^{\frac{1}{2}} \tilde{\mathbf{H}}_j^H \mathbf{w}_k|^2$ are ST l desired and other STs interference signals, respectively. $C = \sum_{k=1}^{K} |\mathbf{h}_r^H \mathbf{w}_j|^2 + \sum_{l=1}^{L} \sum_{k=1}^{K} \xi_j |\boldsymbol{\phi}_{j,r}^H \boldsymbol{\Theta}_j^{\frac{1}{2}} \tilde{\mathbf{H}}_j^H \mathbf{w}_k|^2$ is PRs interference signals.

B. Optimization Problem Formulation

The sum-rate (SMR) maximization problem is given as

$$\begin{aligned} &\underset{\boldsymbol{\Theta}_l, \mathbf{w}_k}{\text{maximize}} \quad \sum_{k=1}^{K} R_{s,k} + \sum_{l=1}^{L} R_{l,r} \\ &\text{subject to} \quad \sum_{k=1}^{K} \|\mathbf{w}_k\|^2 \leq P_S \ \text{(3a)}, \ \ \|\boldsymbol{\Theta}_l\| \leq M_l, \ \text{(3b)}. \end{aligned} \quad (3)$$

The objective function is a non-convex, with $R_{s,k} = \log_2(1+\gamma_{s,k})$ and $R_{l,r} = \log_2(1+\gamma_{s,k})$. Constraint (3a) ensures that the total PT transmit power does not exceed the available power (P_S). Constraint (3b) ensures that $\mathbf{\Theta}_l$ components do not exceed unity. By observation, (3a) is convex with respect to (w.r.t.) $\mathbf{w}_k$. $\mathbf{\Theta}_l$ is an variable w.r.t constraint (3b).

III. Proposed Model-Based Optimization Solution

The solution to the SMR maximization problem is discussed next. First, the $\mathbf{w}_k$ is determined, and then $\mathbf{\Theta}_l$ is defined and used in the proposed alternating optimization (AO) algorithm.

A. Problem Reformulation

Here, the SMR problem is converted to a weighted minimum mean square error (WMMSE) equivalent problem because their sufficient Karush-Kuhn-Tucker (KKT) conditions are similar, and both the SMR and WMMSE problems have the same optimal beamformer solution [8], [13]–[15]. Therefore, the equivalent WMMSE problem is defined as[2]

$$\underset{\{\delta_l,\alpha_l,\mathbf{\Theta}_l\}_{l=1}^{L}\{\rho_k,\beta_k,\mathbf{w}_k\}_{k=1}^{K}}{\text{minimize}} \ \hat{V} \text{ subject to (3a), (3b),} \quad (4)$$

where the MV2X and SNSN WMMSE weights and receive filters are $\{\rho_k, \delta_l\}$ and $\{\beta_k, \alpha_l\}$, respectively, with the WMMSE $\hat{V} = \sum_{k=1}^{K}(\rho_k e_{s,k} - \log(\rho_k)) + \sum_{l=1}^{L}(\delta_l e_{l,r} - \log(\delta_l))$, $e_{l,r} = 1 - \alpha_l \sum_{k=1}^{K}\left(\boldsymbol{\phi}_{l,r}^H \mathbf{\Theta}_l^{\frac{1}{2}} \tilde{\mathbf{H}}_l^H \mathbf{w}_k + \mathbf{w}_k^H \tilde{\mathbf{H}}_l \mathbf{\Theta}_l^{\frac{1}{2}H} \boldsymbol{\phi}_{l,r}\right) + |\alpha_l|^2\left(2\sum_{j=1}^{L}\sum_{k=1}^{K}\xi_j|\boldsymbol{\phi}_{j,r}^H \mathbf{\Theta}_j^{\frac{1}{2}} \tilde{\mathbf{H}}_j^H \mathbf{w}_k|^2 + \sum_{k=1}^{K}|\mathbf{h}_r^H \mathbf{w}_k|^2 + \sigma_r^2\right)$ and $e_{s,k} = 1 + 2|\beta_k|^2 \sum_{l=1}^{L}\sum_{j=1}^{K}\xi_j|\boldsymbol{\phi}_{l,k}^H \mathbf{\Theta}_l^{\frac{1}{2}} \tilde{\mathbf{H}}_l^H \mathbf{w}_j|^2 + |\beta_k|^2 \sum_{j=1}^{K}\xi_j|\mathbf{h}_k^H \mathbf{w}_j|^2 - \beta_k(\mathbf{h}_k^H \mathbf{w}_k + \mathbf{w}_k^H \mathbf{h}_k) + |\beta_k|^2\sigma_k^2 - \sum_{l=1}^{L}\beta_k(\boldsymbol{\phi}_{l,k}^H \mathbf{\Theta}_l^{\frac{1}{2}} \tilde{\mathbf{H}}_l^H \mathbf{w}_k + \mathbf{w}_k^H \tilde{\mathbf{H}}_l \mathbf{\Theta}_l^{\frac{1}{2}H} \boldsymbol{\phi}_{l,k})$.

B. Optimal Resources Determination

Problem (4) is a convex problem w.r.t. all variables. This can be shown from the objective function second derivatives Hessian matrix [8], [14]. Each variable's closed-form solution used in the SMR maximization AO algorithm is found as follows [8], [14]: (i) problem (4)'s Lagrangian is defined, (ii) the first derivative of the Lagrangian w.r.t. the considered variable is equated to zero, and (iii) variable is made the subject, considering that their associated KKT conditions are met.

The weights and receive filters are respectively deduced as

$$\begin{aligned} &\min_{\rho_k} \rho_k e_{s,k} - \log(\rho_k);\ \rho_k = 1/e_{s,k}, \\ &\min_{\delta_l} \delta_l e_{l,r} - \log(\delta_l);\ \delta_l = 1/e_{l,r}, \\ &\min_{\beta_k} e_{s,k};\ \beta_k = \frac{a_k}{\sigma_k^2 + b_k},\ \min_{\alpha_l} e_{l,r};\ \alpha_l = \frac{a_{l,r}}{\sigma_r^2 + b_{l,r}}, \end{aligned} \quad (5)$$

with $b_{l,r} = 2\sum_{j=1}^{L}\sum_{k=1}^{K}\xi_j(|\boldsymbol{\phi}_{j,r}^H \mathbf{\Theta}_j^{\frac{1}{2}} \tilde{\mathbf{H}}_j^H \mathbf{w}_k|^2 + |\mathbf{h}_r^H \mathbf{w}_k|^2)$, $b_k = 2\sum_{l=1}^{L}\sum_{j=1}^{K}\xi_j(|\boldsymbol{\phi}_{l,k}^H \mathbf{\Theta}_l^{\frac{1}{2}} \tilde{\mathbf{H}}_l^H \mathbf{w}_j|^2 + |\mathbf{h}_k^H \mathbf{w}_j|^2)$, $a_{l,r} = \sum_{k=1}^{K}\boldsymbol{\phi}_{l,k}^H \mathbf{\Theta}_l^{\frac{1}{2}} \tilde{\mathbf{H}}_l^H \mathbf{w}_k$, $a_k = \mathbf{h}_k^H \mathbf{w}_k + \sum_{l=1}^{L}\boldsymbol{\phi}_{l,k}^H \mathbf{\Theta}_l^{\frac{1}{2}} \tilde{\mathbf{H}}_l^H \mathbf{w}_k$.

[2]The SMR to WMMSE conversion has been extensively used and can easily be deduced [13]. Hence, the derivation steps were omitted for brevity.

The $\mathbf{w}_k$ beamformer can be determined from

$$\underset{\mathbf{w}_k}{\text{minimize}} \ \hat{V} \text{ subject to (3a), as } \mathbf{w}_k = \mathbf{a}\mathbf{A}^{-1}, \quad (6)$$

where $\mathbf{a} = \mathbf{a}_1 + \mathbf{a}_2$, and $\mathbf{A} = \mathbf{A}_1 + \mathbf{A}_2 + \mathbf{A}_3$ is full-rank, with $\mathbf{a}_1 = \sum_{l=1}^{L}\delta_l\alpha_l\boldsymbol{\phi}_{l,r}^H \mathbf{\Theta}_l^{\frac{1}{2}} \tilde{\mathbf{H}}_l^H$, $\mathbf{A}_1 = \sum_{l=1}^{L}\delta_l|\alpha_l|^2(\mathbf{h}_r\mathbf{h}_r^H + 2\sum_{j=1}^{L}\xi_j(\boldsymbol{\phi}_{j,r}^H \mathbf{\Theta}_j^{\frac{1}{2}} \tilde{\mathbf{H}}_j^H)(\boldsymbol{\phi}_{j,r}^H \mathbf{\Theta}_j^{\frac{1}{2}} \tilde{\mathbf{H}}_j^H)^H)$, $\mathbf{a}_2 = \rho_k\beta_k(\mathbf{h}_k + \sum_{l=1}^{L}\boldsymbol{\phi}_{l,k}^H \mathbf{\Theta}_l^{\frac{1}{2}} \tilde{\mathbf{H}}_l^H)$, $\mathbf{A}_2 = \sum_{j=1}^{K}\rho_j|\beta_j\xi_j|^2(\mathbf{h}_j\mathbf{h}_j^H + 2\sum_{l=1}^{L}(\boldsymbol{\phi}_{l,j}^H \mathbf{\Theta}_l^{\frac{1}{2}} \tilde{\mathbf{H}}_l^H)(\boldsymbol{\phi}_{l,j}^H \mathbf{\Theta}_l^{\frac{1}{2}} \tilde{\mathbf{H}}_l^H)^H)$, $\mathbf{A}_3 = \lambda\mathbf{I}$ and λ is found using a root finding method on (3a) at equality.

Finally, the optimal $\mathbf{\Theta}_l^\star$ is determined from

$$\begin{aligned} &\underset{\mathbf{\Theta}_l}{\text{minimize}} \ \hat{V} \text{ subject to (3b), as} \\ &\mathbf{\Theta}_l = \min\{\hat{A}, \mathbf{I}\},\ \hat{A} = \text{diag}[(\mathbf{A}\mathbf{B}^{-1})(\mathbf{A}\mathbf{B}^{-1})^H] \end{aligned} \quad (7)$$

where variables $\mathbf{A} = \mathbf{A}_1 + \mathbf{A}_2$, $\mathbf{B} = \mathbf{B}_1 + \mathbf{B}_2$, with $\mathbf{B}_2 = 2\sum_{k=1}^{K}\rho_k|\beta_k|^2\sum_{j=1}^{K}\xi_{j,i}(\boldsymbol{\phi}_{l,k}^H \tilde{\mathbf{H}}_l^H \mathbf{w}_j)(\boldsymbol{\phi}_{l,k}^H \tilde{\mathbf{H}}_l^H \mathbf{w}_j)^H$, $\mathbf{A}_1 = \delta_l\alpha_l\sum_{k=1}^{K}\boldsymbol{\phi}_{l,r}^H \tilde{\mathbf{H}}_l^H \mathbf{w}_k$, $\mathbf{A}_2 = \sum_{k=1}^{K}\rho_k\beta_k\boldsymbol{\phi}_{l,k}^H \tilde{\mathbf{H}}_l^H \mathbf{w}_k$, $\mathbf{B}_1 = 2\sum_{k=1}^{K}(\boldsymbol{\phi}_{l,r}^H \tilde{\mathbf{H}}_l^H \mathbf{w}_k)(\boldsymbol{\phi}_{l,r}^H \tilde{\mathbf{H}}_l^H \mathbf{w}_k)^H\sum_{j=1}^{L}\xi_j\delta_j|\alpha_j|^2$.

C. Overhead Analysis

Algorithm 1 SMR maximization with optimal resources

Initialize: $\sum_{k=1}^{K}\|\mathbf{w}_k\|^2 = P_S$, $\|\mathbf{\Theta}_l\|^2 \leq M_l$
repeat
  Update each $\{\rho_k, \delta_l\}$ and $\{\beta_k, \alpha_l\}$ with (5)
  Update each $\mathbf{\Theta}_l$ and $\mathbf{w}_k$ with (7) and (6)
until SMR convergence

The proposed SMR maximization AO algorithm is presented in Algorithm 1, which is implemented at the PT and has a computational complexity of $\mathcal{O}(I_I[L^4+K^4]+\log(1/\epsilon))$ for the arithmetic determination of the 3 MV2X and 3 SNSN variables, SMR and the convergence criteria ϵ. I_I represents the iteration computational complexity. Algorithm 1 converges to an optimum solution. The optimality is achieved because the resource allocation solutions satisfy the Lagrangian and the KKT conditions. Hence, fulfilling the Lagrangian and KKT conditions meets the first necessary, sufficient conditions for optimality [8], [14], [15]. The solution is shown to satisfy the second-order necessary condition (SONC) and second-order sufficient condition (SOSC) by deriving the Hessian matrix (second derivatives) w.r.t. all variables from the WMMSE problem and equations [8], [14], [15]. From the discussion on SNSC, with each iteration, the acquired $\text{SMR}^{n+1}(\mathbf{w}_k, \mathbf{\Theta}_l) > \text{SMR}^{n}(\mathbf{w}_k, \mathbf{\Theta}_l)$, for iteration number n until the optimal point is reached where $\text{SMR}^{n}(\mathbf{w}_k, \mathbf{\Theta}_l) \approx \text{SMR}^{n-1}(\mathbf{w}_k, \mathbf{\Theta}_l)$ and $\text{SMR}^{n}(\mathbf{w}_k^\star, \mathbf{\Theta}_l^\star) - \text{SMR}^{n-1}(\mathbf{w}_k^\star, \mathbf{\Theta}_l^\star) \leq \epsilon$ is satisfied, with ϵ being the convergence criteria.

IV. Algorithm Evaluation and Discussion

Simulation Setup and Topology Discussions: The simulation set-up and variable values are presented in Table I and an example of the 2D topology displayed in Fig. 2(a) [16]. The 2D simulation urban environment is modelled using the V2X

TABLE I
SIMULATION VARIABLE DEFINITIONS AND VALUES.

Variable	Value	Variable	Value	Variable	Value	Variable	Value	Variable	Value
$\hat{h}_{\text{PT}}$	25m	$\hat{h}_{\{\text{ST,SR}\}}$	23m	v	3Km/h	C	3×10^8m/s	f_c	2.4×10^9Hz
ϵ_x	0.988	(σ_e^2, ξ_x)	$(10^{-3}, 10^{-5})$	$(\rho, \eta_{m,l})$	$(4, 0.5)$	N	40	K	8
P_S	20dBm	σ_k^2	-130dBm	σ_r^2	-130dBm	T	5ms	(L, M_l)	$(6, 60)$

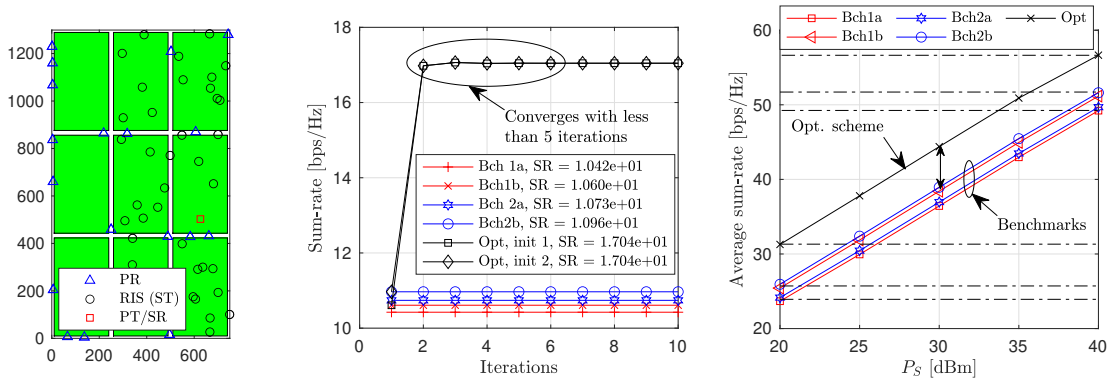

(a) (b) (c)

Fig. 2. (a) 2D urban grid example, (b) Convergence of Algorithm 1, and (c) Average sum-rate vs increasing PT power.

standards and depicted in 2(a). For the building, PT antenna, PR, ST and SR height ($\hat{h}_x$) are also acquired from the V2X and cellular urban macro scenario (UMa) standards documentation [16]. The UMa pathloss model is used as large-scale fading, and Rician fading ($\sqrt{\rho/\rho+1}\varepsilon^{\text{L}} + \sqrt{1/\rho+1}\varepsilon^{\text{NL}}$) with Rician factor ($\rho$), line-of-sight (L) ($\varepsilon^{\text{L}}$) and non-L (NL) ($\varepsilon^{\text{NL}}$)) is used the for small-scale fading component of the channel modelling [8]. The UMa model is defined as

$$\text{PL(UMa-L)} = \begin{cases} \text{PL}_1(10\text{m} \leq d_{\text{2D}} \leq d_{\text{BP}}), \\ \text{PL}_2(d_{\text{BP}} \leq d_{\text{2D}} \leq 5\text{km}), \end{cases} \quad \text{and} \quad (8)$$
$$\text{PL(UMa-NL)} = \max(\text{PL(UMa-L)}, \text{PL}_3),$$

where $\text{PL}_1 = 28.0 + 22\log_{10}(d_{\text{3D}}) + 20\log_{10}(f_c)$, $\text{PL}_2 = 28.0 + 40\log_{10}(d_{\text{3D}}) + 20\log_{10}(f_c) - 9\log_{10}((d_{\text{BP}})^2 + (\hat{h}_x - \hat{h}_x)^2)$, $\text{PL}_3 = 13.54 + 39.08\log_{10}(d_{3D}) + 20\log_{10}(f_c) - 0.6(\hat{h}_x - 1.5)$, and d_{2D}, d_{3D}, d_{BP} are the inter-node 2D, 3D and breakpoint distances, respectively [16]. (i) Zero-forcing (ZF) beamformer with fixed (Bch1a) and optimal (Bch1b) $\mathbf{\Theta}_k$, and (ii) maximum ratio transmission (MRT) beamformer with fixed (Bch2a) and optimal (Bch2b) $\mathbf{\Theta}_k$ [8], [17] are used as benchmarks, with 10^3 random channels per figure.

Algorithm Convergence and Performance Discussions: Fig. 2(b) shows the convergence of the Opt. scheme with two randomized initialization (i.e., init 1: ZF $\mathbf{w}_k$ and randomized $\mathbf{\Theta}_l$, and init 2: MRT $\mathbf{w}_k$ and randomized $\mathbf{\Theta}_l$), and the convergence of the benchmarks schemes (i.e., Bch1a, Bch1b, Bch2a and Bch2b). From Fig. 2(b), Opt init 1 and init 2 have different starting points but converge to the same optimum sum-rate value of 17bps/Hz after about 5 algorithm iterations. However, the benchmark schemes have constant sum-rate values with increasing iterations because the $\mathbf{w}_k$ and $\mathbf{\Theta}_l$ are determined initially and remain unchanged during the iterations. As PT transmit power increases, the sum-rate performance is shown in Fig. 2(c). From Fig. 2(c), the sum-rate increases with increasing P_S for all schemes, with the Opt scheme having the best performance. This behavior is observed because of the small imperfection factors ($(\sigma_e^2, \xi_x, \epsilon) = (10^{-3}, 10^{-5}, 0.9881]$), near perfect system) considered within the simulations. The Opt schemes outperform the nearest benchmark scheme (Bch2b) by about 6bps/Hz, while the difference between the individual ZF (i.e., Bch1a and Bch1b) and MRT (i.e., Bch2a and Bch2b) benchmark schemes is 1bps/Hz. Next, discussions on how the system imperfections affect sum-rate performance are presented.

Imperfections Influence Discussions: Figs. 3(a) and 3(b) show how the sum-rate is affected by increased imperfections in both SIC and CSI, respectively. From both plots, it is observed that the sum-rate deteriorates as the imperfection factor increases. From Fig. 3(a), at the imp-SIC factor increases, the sum-rate reduces because the interference components within the SINR increase, leading to a reduction in individual rates, which affects the sum-rate achieved. When $\xi_x \approx 1$, there is no SIC performed within the system model. Even with no SIC performed, the Opt scheme has a significant sum-rate of 10bps/Hz over the benchmark schemes. While with near perfect SIC performed within the system model, the difference reduces to approximately 5bps/Hz. This shows that the proposed algorithm is robust whether or not SIC is used within the symbiotic radio framework. Fig. 3(b) gives inferences on the sum-rate performance with imp-CSI estimation due to estimation protocol imperfections. As expected, the sum-rate reduced with increasing imp-CSI variance. This increase in imperfections leads to errored, desired signal estimation, affecting the interference within the estimated data. Hence, this leads to a reduction in the individual rates, then a decrease

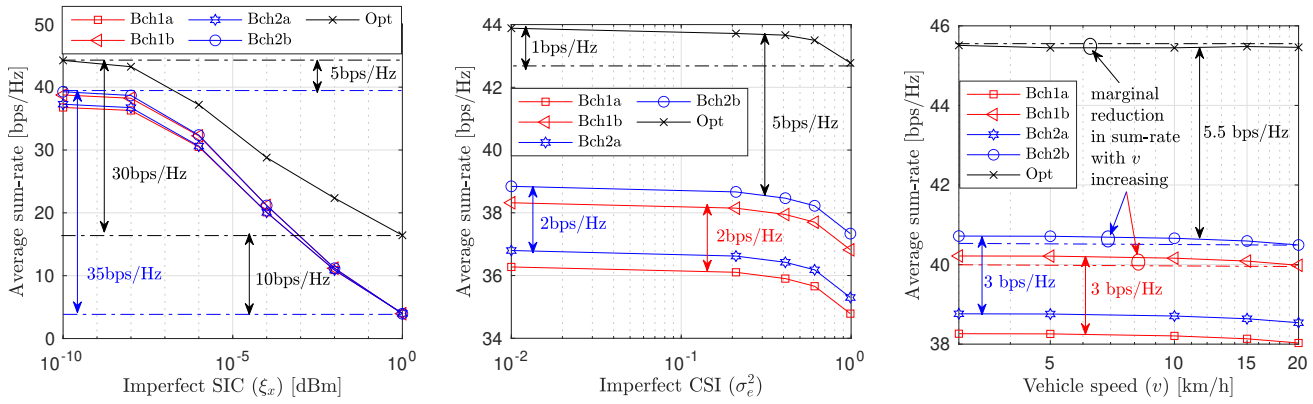

(a) (b) (c)

Fig. 3. Average sum-rate versus (a) imp-SIC factor, (b) imp-CSI factor, and (c) vehicle speed.

in the sum-rate achieved. The constant 5bps/Hz between the Opt scheme and Bch2b is maintained, while the 2bps/Hz performance difference is present between the ZF (Bch1a and Bch1b) and the MRT (Bch2a and Bch2b) schemes.

To determine the influence of imp-CSI estimation due to the effects of vehicle speed on the sum-rate achieved is illustrated in Fig. 3(c). As the vehicle's speed increases, the ϵ_x factor reduces for each vehicle interaction channel gains (i.e., between PT-to-PRs and ST-to-PRs link). Therefore, the PN (i.e., PRs) rate decreases, while the SN (i.e., STs received signal) rates remain constant. This leads to a slight reduction in the sum-rate as observed in Fig. 3(c). The reduction in the Opt. scheme is smaller than that of the benchmark schemes due to its more robust dynamic beamforming and reflection coefficient adaptation for the instantaneous channels compared to the more adaptive benchmark schemes. There are constant performance differences between the schemes. There is an approximate 0.5bps/Hz between the MRT and ZF benchmarks, and an approximate 3bps/Hz performance difference between Bch1a and Bch1b, with similar difference between Bch2a and Bch2b. The Opt. scheme has an approximate performance of 5.5bps/Hz, better than the closest benchmark scheme (Bch2b). Hence, with the optimal resource allocation for sum-rate maximization, the proposed scheme is robust to changing v.

V. Conclusion

This paper investigated the symbiotic relationship between an MV2X PN and a multi-RIS BackCom SN, focusing on joint resource optimization to maximize system SR. We developed an alternating algorithm to maximize the SR and jointly optimize the resource allocation, showing superiority over conventional equal resource allocation schemes in the system simulations. Future considerations are joint sensing and communication integration and MIMO architecture.

References

[1] L. Zhang, M. Xiao, G. Wu, M. Alam, Y.-C. Liang, and S. Li, "A survey of advanced techniques for spectrum sharing in 5G networks," *IEEE Wireless Commun.*, vol. 24, no. 5, pp. 44–51, Oct. 2017.

[2] W. U. Khan, T. N. Nguyen, F. Jameel, M. A. Jamshed, H. Pervaiz, M. A. Javed, and R. Jäntti, "Learning-based resource allocation for backscatter-aided vehicular networks," *IEEE Trans. Intelligent Transportation Sys.*, vol. 23, no. 10, pp. 19 676–19 690, Nov. 2021.

[3] D. Darsena, G. Gelli, and F. Verde, "Modeling and performance analysis of wireless networks with ambient backscatter devices," *IEEE Trans. Commun.*, vol. 65, no. 4, pp. 1797–1814, Jan. 2017.

[4] H. Zhou, X. Kang, Y.-C. Liang, S. Sun, and X. Shen, "Cooperative beamforming for reconfigurable intelligent surface-assisted symbiotic radios," *IEEE Trans. Veh. Technol.*, vol. 71, no. 11, pp. 11 677–11 692, Jul. 2022.

[5] Q. Zhang, Y.-C. Liang, and H. V. Poor, "Reconfigurable intelligent surface assisted MIMO symbiotic radio networks," *IEEE Trans. Commun.*, vol. 69, no. 7, pp. 4832–4846, Mar. 2021.

[6] X. Xu, Y.-C. Liang, G. Yang, and L. Zhao, "Reconfigurable intelligent surface empowered symbiotic radio over broadcasting signals," *IEEE Trans. Commun.*, vol. 69, no. 10, pp. 7003–7016, Jun. 2021.

[7] J. Hu, Y.-C. Liang, and Y. Pei, "Reconfigurable intelligent surface enhanced multi-user MISO symbiotic radio system," *IEEE Trans. Commun.*, vol. 69, no. 4, pp. 2359–2371, Dec. 2020.

[8] D. K. P. Asiedu and J.-H. Yun, "Multiuser NOMA with multiple reconfigurable intelligent surfaces for backscatter communication in a symbiotic cognitive radio network," *IEEE Trans. Veh. Technol.*, vol. 72, no. 4, pp. 5300–5316, Apr. 2023.

[9] J. Wang, H.-T. Ye, X. Kang, S. Sun, and Y.-C. Liang, "Cognitive backscatter NOMA networks with multi-slot energy causality," *IEEE Commun. Let.*, vol. 24, no. 12, pp. 2854–2858, Aug. 2020.

[10] H. Li, Y. Zhang, and B. Clerckx, "Channel estimation for beyond diagonal reconfigurable intelligent surfaces with group-connected architectures," in *Proc. IEEE Int. Workshop Computational Advances in Multi-Sensor Adaptive Processing*. IEEE, Dec. 2023, pp. 21–25.

[11] O. Dizdar, Y. Mao, and B. Clerckx, "Rate-splitting multiple access to mitigate the curse of mobility in (massive) MIMO networks," *IEEE Trans. Commun.*, vol. 69, no. 10, pp. 6765–6780, Jul. 2021.

[12] Y. Zhao and B. Clerckx, "RIScatter: Unifying backscatter communication and reconfigurable intelligent surface," *IEEE J. Sel. Areas Commun.*, vol. 42, no. 6, pp. 1642–1655, Apr. 2024.

[13] S. S. Christensen, R. Agarwal, E. De Carvalho, and J. M. Cioffi, "Weighted sum-rate maximization using weighted MMSE for MIMO-BC beamforming design," *IEEE Trans. Wireless Commun.*, vol. 7, no. 12, pp. 4792–4799, Dec. 2008.

[14] E. K. Chong and S. H. Zak, *An introduction to optimization*. John Wiley & Sons, Jan. 2013, vol. 75.

[15] S. Boyd, S. P. Boyd, and L. Vandenberghe, *Convex optimization*. Cambridge university press, 2004.

[16] 3GPP, "TR 38.901 V17.0.0: Study on channel model for frequencies from 0.5 to 100 GHz, (Release 17)," pp. 26–29, Mar. 2022.

[17] S. Kiani, M. Dong, S. ShahbazPanahi, G. Boudreau, and M. Bavand, "Learning-based user clustering in NOMA-aided MIMO networks with spatially correlated channels," *IEEE Trans. Commun.*, vol. 70, no. 7, pp. 4807–4821, 2022.